Cylindrical Sound Wave Generated by Shock-Vortex Interaction

Herbert S. Ribner*
University of Toronto, Downsview, Canada
and
NASA Langley Research Center, Hampton, Virginia

The passage of a columnar vortex broadside through a shock is investigated. This has been suggested as a crude, but deterministic, model of the generation of "shock noise" by the turbulence in supersonic jets. The vortex is decomposed by Fourier transform into plane sinusoidal shear waves disposed with radial symmetry. The plane sound waves produced by each shear wave/shock interaction are recombined in the Fourier integral. The waves possess an envelope that is essentially a growing cylindrical sound wave centered at the transmitted vortex. The pressure jump across the nominal radius $R=ct$ attenuates with time as $R^{-1/2}$ and varies around the arc in an antisymmetric fashion resembling a quadrupole field. Very good agreement, except near the shock, is found with the antisymmetric component of reported interferometric measurements in a shock tube. Beyond the front $r\simeq R$ is a *precursor* of opposite sign, that decays like R^{-1}, generated by the $1/r$ potential flow around the vortex core. The present work is essentially an extension and update of an early approximate study at $M=1.25$. It covers the range (R/core radius) = 10, 10^2, 10^3, and 10^4 for $M=1.25$ and (in part) for $M=1.29$ and, for fixed (R/core radius) = 10^3, the range $M=1.01$ to ∞.

Nomenclature

a	= radius of vortex core upstream of shock
b	∝ local thickness of cylindrical wave front, varies with α'' or ϕ'' (Fig. 5)
c_A	= speed of sound upstream of shock
c	= speed of sound downstream of shock
G	$= G[(r''-R)/b(\phi''); R/a; \phi'']$, function describing (primarily) radial distribution of pressure in cylindrical sound wave (not to be confused with $G=-\cot\alpha''$ in Appendix)
k,k',k''	= wave number vectors (k,α), (k',α'), (k'',α''), respectively ⊥ phase lines of dq, dq', and dp in Fig. 2
J	= Jacobian, $\partial\alpha/\partial\alpha''$ (see Appendix)
K_s	$= 2q_{max}/\pi U_A$, normalized vortex strength
M	$= U_A/c_A$, Mach number upstream of shock
M_1	$= U/c$, Mach number downstream of shock
$\hat{P}$	= nondimensional transfer function relating dp to dq
p	= pressure perturbation/ambient pressure at (r'',ϕ'')
q_{max}	$= \Gamma/2\pi a$, peak velocity in vortex field when upstream of shock
R	$= ct$, nominal radius of cylindrical sound wave
r,ϕ	= cylindrical coordinates of field point for incident shear waves
r'',ϕ''	= cylindrical coordinates of field point for pressure waves
U_A	= flow velocity upstream of shock
U	= flow velocity downstream of shock
W	= a virtual velocity defined in Fig. 4; condition $W<$ sound speed ($\alpha'>\alpha'_{cr}$) yields evanescent pressure waves
Γ	= circulation about core of columnar vortex when upstream of shock
σ	$= (r''-R)/b(\phi'')$, normalized radial coordinate

Received Sept. 19, 1984; revision received Jan. 22, 1985.

*Professor, Institute for Aerospace Studies.

Introduction

THERE has been renewed interest in a problem studied by Hollingsworth and Richards[1,2] over a quarter century ago. It is considered to be a crude, but deterministic, model of the generation of "shock noise"[3-6] by turbulence passing through the shock wave pattern of a supersonic jet. In this idealization, a columnar vortex passes broadside through a planar shock wave; a cylindrical sound wave appears on the downstream side, partly cut off by the shock. This is centered on the moving vortex core and both grows and convects; these features are clearly visible in schlieren photos (e.g., Fig. 1) and interferograms taken in a shock tube.[7]

The theory of oblique shear wave/shock interaction developed by the present author[4,8] (see also Refs. 9-11 and later studies) formed the basis of two predictive analyses[2,12] at that time. The more elaborate of these, by Ram and Ribner,[12] showed rough agreement with the pressure discontinuity around the cylindrical wave front measured by Dosanjh and Weeks.[7] A still more elaborate theory, an extension of the formalism of Lighthill[13] and Curle,[14] was developed by Weeks and Dosanjh.[15] It yielded astonishing agreement with the cited experiment but, unlike Ref. 12, provided no quantitative information on radial pressure profiles.

The problem was revisited in 1981 by Pao and Salas[16] via a numerical solution of the Euler equations. The related problem of the interaction of a hot spot with a shock has also been treated by such an approach.[17] The numerical techniques for spatial problems are still evolving and there remain questions of accuracy in terms of resolution, sensitivity to imposed artificial boundary conditions, etc. This has stimulated new interest in the analytical approach on our part. As will be seen, this can provide further insights as well as comparative results.

Our 1957-59 study[12] was in part approximate; it led to what were thought to be the upper and lower bounds for the radial pressure profiles. The approximation, motivated by difficulties of analytical integration, can nowadays be removed by computerized numerical integration. Extensive computations of this kind have been carried out and form the basis of the present paper. It may be regarded as an extended and updated version of the earlier work. The new predicted results are again compared with experiment.

Overview

The interaction of an inclined sinusoidal shear wave with a shock gives rise to a refracted shear-entropy wave and a pressure wave,[7-11] also sinusoidal (Fig. 2a). (The pressure waves are of two kinds, depending on the angle of $\overline{dq}$: *evanescent* waves that decay with distance from the shock and *nonevanescent* waves that do not decay.) These sine waves may be superposed in Fourier integrals to yield the interaction of waves of arbitrary profile with a shock.

A particular example is shown in Fig. 2b. Suppose now that infinitely many weak shear waves of this special profile are uniformly distributed radially like the spokes of a wheel; then the resultant velocity field is that of a vortex of core radius a (Fig. 3a). This can be demonstrated formally in terms of a two-dimensional Fourier integral.

If the vortex is convected the constituent shear waves are convected (Fig. 3b). The geometry before and after encountering a shock, omitting the sound waves, is such as to bring the waves to a focus in the "after" interaction sketch. This focus can be interpreted as the core center of the transmitted modified vortex. (This core is oval shaped, characterized by an angle-dependent radius b.)

In Fig. 4a we look at the "after" interaction shear waves and limit attention to inclinations with the shock less than a certain angle α'_{cr}. The centerlines of the sound waves due to the shock interaction are now added. These plane waves are of the *nonevanescent* kind; they come off from the shock at the proper positions and angles so as to combine into a cylindrical envelope of radius $R = ct$.

Figure 4b clarifies the formation of the envelope. Let U be the subsonic stream velocity downstream of the shock and t be the time (t is taken as zero when the core center transits the shock). Then W is a supersonic velocity determined by the inclination α' of the shear wave and μ is the Mach angle associated with that velocity, according to Refs. 4 and 8. The relation $\sin\mu = c/W$ then requires the distance from the vortex core to the sound wave to equal ct. This distance remains constant at ct for all the sound waves, even though W changes with the shear wave inclination. Thus, the centerlines of the special profile sound waves are tangent to a circle of radius $R = ct$ (Fig. 4a).

The strength of the sound pressure field maximizes rather sharply close to this circle or, rather, circular cylinder of tangency: the effect is that of a cylindrical sound wave. The pressure varies around the circumference of the wave, being dominated at any point by the contribution of the plane waves tangent near that point. Since the plane waves are

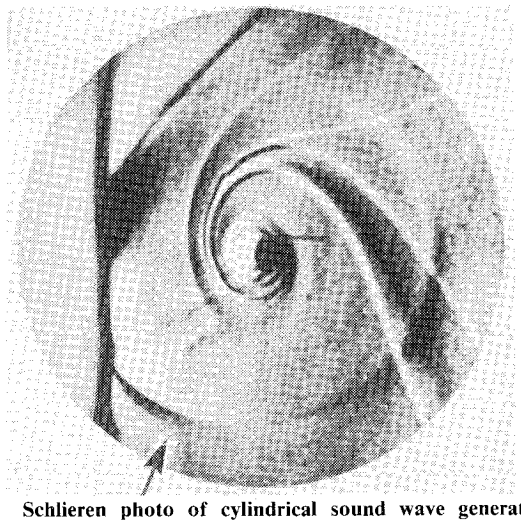

Fig. 1 Schlieren photo of cylindrical sound wave generated by passage of vortex through Mach 1.29 shock wave. (Unpublished photo from files of Ref. 7 research, courtesy of Dr. Dosanjh.)

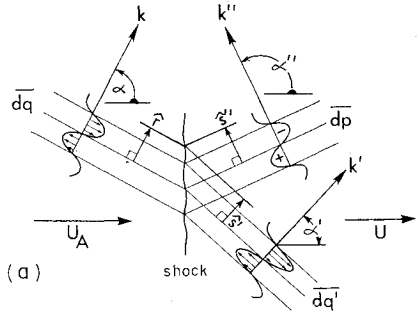

Fig. 2a Interaction of a sinusoidal shear flow with a shock.

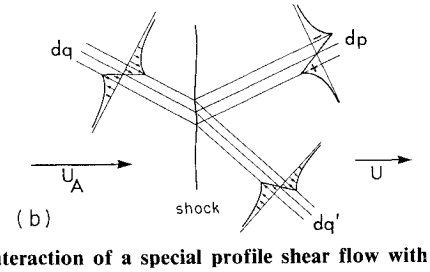

Fig. 2b Interaction of a special profile shear flow with a shock.

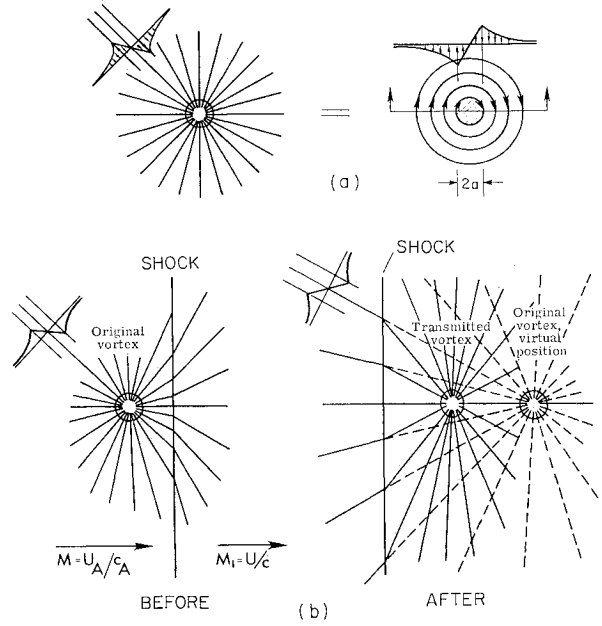

Fig. 3 a) Synthesis of vortex from radially disposed special profile shear flows (physical interpretation of Fourier integral); b) Convection of vortex through shock wave. "Focus" of refracted shear waves is transmitted vortex.

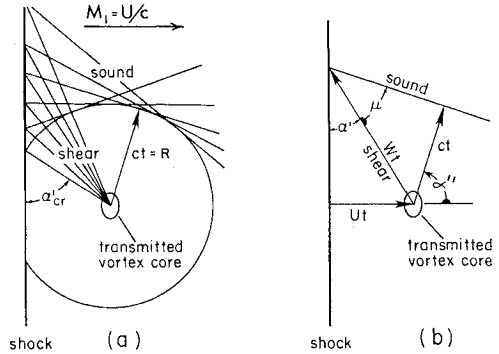

Fig. 4 Convection of vortex through a shock. Nonevanescent sound waves generated at shock (Fig. 2) are added to shear waves of Fig. 3b: a) formation of envelope of radius ct; b) geometric basis and definition of virtual velocity W.

spread more thinly as the radius R grows with time, the pressure diminishes; it turns out that the pressure *jump* at R varies inversely as the square root of R.

For transmitted shear wave angles α' greater than α'_{cr} (Fig. 4), the velocity W is *subsonic* (as is the graphical construct c, now to be labeled c_E, which is no longer the speed of sound). Then different angular relations hold for the pressure waves and they decay exponentially with distance downstream of the shock. These *evanescent* waves do not coelesce to an envelope and will not contribute to the pressure jump at R. Their contribution is briefly discussed, but omitted from the calculated curves. By definition, the transition from supersonic to subsonic W occurs at the critical shear wave inclination α'_{cr}. Thus, the pressure integrals of the *nonevanescent* waves of Fig. 4 are limited herein to the angular range $0 \leq |\alpha'| \leq \alpha'_{cr}$ of the associated shear waves.

Analysis

Resolution of Vortex into Oblique Shear Waves

The velocity field of a columnar vortex of core radius a and clockwise circulation 2π is given by

$$\begin{array}{lll} & \underline{R<a} & \underline{R>a} \\ u(r,\phi) = & (r/a^2)\sin\phi & (1/r)\sin\phi \\ v(r,\phi) = & -(r/a^2)\cos\phi & -(1/r)\cos\phi \end{array} \qquad (1)$$

where r is measured radially from the vortex center. A two-dimensional Fourier development can be obtained in the form

$$u(r,\phi) = \frac{2}{\pi}\int_{-\pi/2}^{\pi/2}\sin\alpha\,d\alpha\int_0^\infty \frac{J_1(ka)}{ka}\sin k\hat{r}\,dk$$

$$v(r,\phi) = -\frac{2}{\pi}\int_{-\pi/2}^{\pi/2}\cos\alpha\,d\alpha\int_0^\infty \frac{J_1(ka)}{ka}\sin k\hat{r}\,dk \qquad (2)$$

where $\hat{r} = r\cos(\alpha-\phi)$.

The integrands can be interpreted as the velocity components du, dv in an elementary sinusoidal shearing flow (shear wave) dq (Fig. 2a) with normal inclined at an angle α with the horizontal; $\hat{r}$ is the variable describing planes of constant phase. If the vortex circulation is generalized from 2π to Γ, the resultant velocity in this wave may be written as

$$\overline{dq}/U_A = (\Gamma/U_A\pi^2 ka^2)J_1(ka)\sin k\hat{r}\,d(ka)\,d\alpha \qquad (3)$$

in nondimensional form.

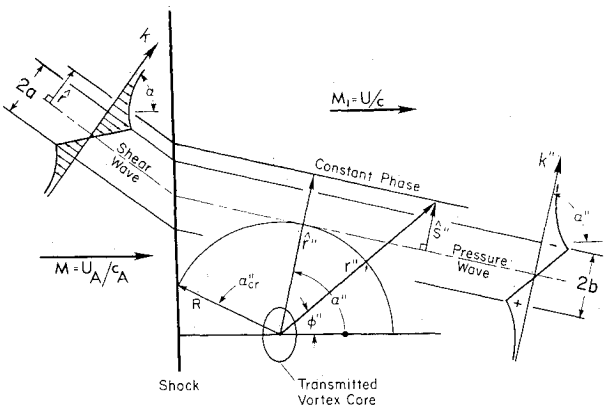

Fig. 5 Reversion to elementrary shear wave→pressure wave/shock interaction of Fig. 2b, with more detail. (In Figs. 3, 4 waves like these, with a range of angles α and corresponding α'', are superposed.)

Pressure Wave from Shear Wave/Shock Interaction

Interaction of the shear wave with the shock (Fig. 2a) gives rise to pressure wave of different inclination α'' and wave knumber k'',[4,8]

$$\overline{dp} = -\hat{P}(\Gamma/U_A\pi^2 ka^2)J_1(ka)\sin(k''\hat{s}'' - \delta_p)\,d(ka)\,d\alpha \qquad (4)$$

where the phase variable $\hat{s}''$ is defined in Fig. 2a compatibly with $\hat{r}$. Here p signifies pressure perturbation divided by ambient pressure p_∞. The transfer function $\hat{P}$ (see Appendix), with its possible phase shift δ_p, describes quantitatively the relation between the pressure wave and shear wave of Fig. 2a.

It will be convenient to recast Eq. (4) in terms of k'' and α'' rather than k and α. To this end we write

$$d(ka)\,d\alpha = J(\alpha'')\,d(k''b)\,d\alpha'' \qquad (5)$$

where $J(\alpha'')$ is the Jacobian $\partial\alpha/\partial\alpha''$, with functional form given in the Appendix. The length b is chosen to make $k''b = ka$; it is given a geometric interpretation at a later stage (Fig. 5). Furthermore, compatibility of the wave traces of dq and dp along the shock requires that $k''\sin\alpha'' = k\sin\alpha$.

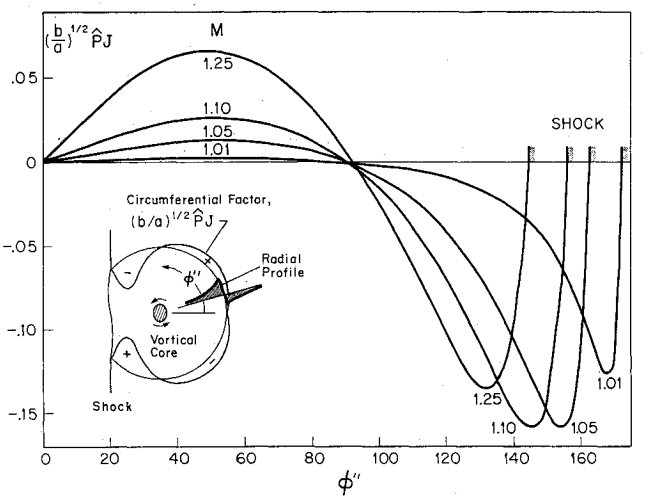

Fig. 6a Variation with ϕ'' of amplitude of radial sound pressure profile (upstream $M = 1.01, 1.05, 1.10, 1.25$).

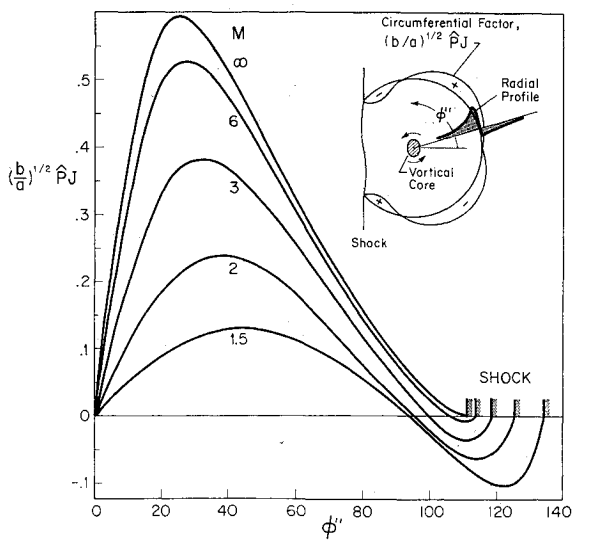

Fig. 6b Variation with ϕ'' of amplitude of radial sound pressure profile (upstream $M = 1.5, 2, 3, 6, \infty$).

These relations are combined as

$$b/a = k/k'' = \sin\alpha''/\sin\alpha \tag{6}$$

The integral of Eq. (3) from 0 to ∞ in ka can be evaluated in closed form.[18] The corresponding integral of Eq. (4), using Eq. (5), in $k''b$ can be evaluated similarly (but only for a certain range of α'' for which $\hat{P}$ is independent of k'' and $\delta_p = 0$). The result is

$$dp = -\hat{P}(\Gamma/U_A\pi^2 a)g(\rho)J(\alpha'')da \tag{7}$$

where

$$\left.\begin{aligned} g(\rho) &= \rho \qquad |\rho| \le 1 \\ &= [\rho + (\rho/|\rho|)\sqrt{\rho^2-1}]^{-1} \qquad |\rho| \ge 1 \\ \rho &\equiv \hat{s}''/b(\alpha'') = (\hat{r}'' - R)/b(\alpha'') \\ \hat{r}'' &\equiv r''\cos(\alpha'' - \phi'') \\ \sigma &\equiv \rho_{\alpha''=\phi''} \equiv (r'' - R)/b(\phi'') \end{aligned}\right\} \tag{8}$$

Equations (7) and (8) describe *the special pressure profile* shown on the upper right of Fig. 2b. [The special profile of dq on the left of Fig. 2b is of similar form, with ρ replaced by $\rho_A = \hat{r}/a(\alpha)$ in $g(\rho)$.]

Superposition of Pressure Waves

A second integration, this time over inclination α'', is called for: this superposes pressure waves (sound waves) as shown schematically in Fig. 4a. The limits of integration $-\alpha''_{cr} \le \alpha'' \le \alpha''_{cr}$ are chosen to exclude the waves for which Eq. (7) is invalid (see above); these are the so-called evanescent waves that decay exponentially with distance downstream of the shock, at a rate governed by k''. This integral describes the contribution of *nonevanescent* waves to the (nondimensional) pressure perturbation p at a point (r'',ϕ'') downstream of the shock. It takes the form

$$\frac{p(r'',\phi'')}{K_s} = \int_{-\alpha''_{cr}}^{\alpha''_{cr}} \hat{P}(\alpha'')J(\alpha'')g(\rho)d\alpha'' \tag{9}$$

with

$$K_s = 2q_{max}/\pi U_A$$

Herein ρ depends on r'', ϕ'', and α'' (right-hand side of Fig. 5) in terms of parameters σ and R/a; σ is the radial distance from the nominal radius $R = ct$ of the cylindrical wave envelope normalized by b, which depends on ϕ''. α''_{cr} is the critical value of wave normal inclination at which W (defined in Fig. 4b) equals the sound speed c (or $\bar{W} \equiv W/c = 1$).

A more detailed derivation leading essentially to Eqs. (8) and (9) is given in Ref. 12. It involves an intermediate transfer of origin to a point on the shock, which clarifies the geometric basis of Eq. (4).

The transfer function $\hat{P}(\alpha'')$ has been defined herein only for the positive (counterclockwise) range of α''. The antisymmetry of the vortex flow ensures that the integrand of Eq. (9) is likewise antisymmetric in α''. Thus, the integration in Eq. (9) may be limited to positive α with the equation reformulated as follows:

$$\frac{p(r'',\phi'')}{K_s} = -\int_0^{\alpha''_{cr}} \hat{P}(\alpha'')g(\rho)_{\phi''}d\alpha'' + \int_0^{\alpha''_{cr}} \hat{P}(\alpha'')J(\alpha'')g(\rho)_{-\phi''}d\alpha'' \tag{10}$$

In the second integral, ρ [defined in Eq. (8)] is evaluated at angle $-\phi''$ rather that at ϕ''.

Reference 12 carried out an approximate analytic integration of Eq. (10) applicable for large nominal sound wave radius ($R/a \to \infty$). The function $g(\rho)$ is then very localized; it was approximated, after normalization, by a δ function. This led very simply, with some approximation, to analytically determined upper and lower bounds to $p(r'',\phi'')/K_s$. Evaluation was for a single Mach number, $M = 1.25$.

Herein the integration of Eq. (10) has been carried out numerically, without the prior approximations, and there are other extensions. Values of the nominal cylindrical sound wave radius R were taken as $R/a = 10$, 10^2, 10^3, and 10^4 (the last value corresponds loosely to the $R/a \to \infty$ bounds of Ref. 12). All four cases were evaluated for $M = 1.25$ and the first three for a wide range of M.

Format of Predictive Equations

The *large radius approximation* ($R/a \to \infty$) made in Ref. 12 does have the great virture of simplicity, in both the analysis and the form of the results. The pressure field comes out in the asymptotic form

$$p = 2^{1/2}K_s \underbrace{\left(\frac{a}{R}\right)^{1/2}}_{\text{const (for fixed } R=ct)} \underbrace{\tilde{G}\left(\frac{r''-R}{b(\phi)}\right)}_{\text{radial}} \underbrace{\left(\frac{b}{a}\right)^{1/2}_{\phi''} P(\phi'')J(\phi'')}_{\text{circumferential}} \tag{11}$$

that is, the product of *unique* circumferential and radial factors for a given shock strength. On dropping the $R/a \to \infty$ approximation (present numerical work), the factorization does not appear. The general result [Eq. (10)] can, however, be rewritten so that it formally resembles Eq. (11) as

$$p = 2^{1/2}K_s \underbrace{\left(\frac{a}{R}\right)^{1/2}}_{\text{const}} \underbrace{G\left(\frac{r''-R}{b(\phi'')};\frac{R}{a};\phi''\right)}_{\text{radial}} \underbrace{\left(\frac{b}{a}\right)^{1/2}_{\phi''} P(\phi'')J(\phi'')}_{\text{circumferential}} \tag{12}$$

by defining a nondimensional radial pressure profile as

$$G\left(\frac{r''-R}{b(\phi'')};\frac{R}{a};\phi''\right) \equiv \frac{p[\text{Eq. (10)}]}{2^{1/2}K_s(a/R)^{1/2}(b/a)^{1/2}_{\phi''}\hat{P}(\phi'')J(\phi'')} \tag{13}$$

To *summarize*, Eqs. (12) and (13) are based on the numerically evaluated integral of Eq. (10); they describe the cylindrical sound wave resulting from passage of a vortex through a shock wave. The circumferential factor is *defined* to be unique. The radial pressure profile G, unlike $\tilde{G}$, is not unique: it depends on both R/a and ϕ'' for a given flow Mach number. But we shall see an approach to uniqueness in certain plots. The parameter $R = ct$ is the nominal radius of the wave, a is the initial vortex core radius, and the constant K_s is a measure of the vortex strength; G, b/a, $\hat{P}$, and J all show some dependence (small for G) on upstream flow Mach number M or, equivalently, on shock strength.

Circumferential Pressure Profile

The circumferential factor $(b/a)^{1/2}\hat{P}J$ is plotted vs ϕ'' in Fig. 6 for a range of upstream Mach numbers from 1.01 to ∞. The sign is reversed to correspond to counterclockwise vorticity, as in the experiments to be compared with. The curves are antisymmetric, and only the positive range of ϕ'' is shown for best detail. The quadrupole-like pressure variation from (+) to (−) to (+) to (−) is striking; this alternation can be seen clearly on the experimental schlieren photograph of Fig. 1. A typical radial pressure profile is shown in the inset sketch of Fig. 6; it makes clear the meaning of the nominal radius R.

Radial Pressure Profile

Variation with Flow Mach Number

Radial pressure profiles $G[(r''-R)/b(\phi''); R/a; \phi'']$ are shown for the same wide range of upstream Mach numbers in Fig. 7; $(r''-R)/b(\phi'')$ is designated by the symbol σ. These apply to the "far-field" or large-time condition $R/a=1000$; they are evaluated for M at the value of ϕ'' at which the circumferential amplitude $(b/a)^{1/2}\hat{P}J$ reaches its first maximum in absolute value. Note that there is a virtual collapse of the profiles into a *single curve*. More precisely, an almost invariant radial profile is displaced slightly upward as M increases from 1.01 to 1.5, being approximately at the asymptote from $M=1.5$ to ∞. In all cases, the jump in G (normalized "strength" of the sound wave) *remains constant* at $\Delta G=2.19$ to three significant figures.

The approximate single curve collapse in terms of σ is a bit misleading. Physically the profiles *vary* in width with ϕ''; the collapse is due to the parameter σ: this equals the radial increment $r''-R$ scaled with the *variable* length parameter $b(\phi'')$. For $M=1.25$, the ratio of $b(\phi'')$ to the original vortex core radius a varies more than twofold: from 1.56 at $\phi''=0$ down to 0.56 at $\phi''=144.35$ deg $=\phi''_{cr}$.

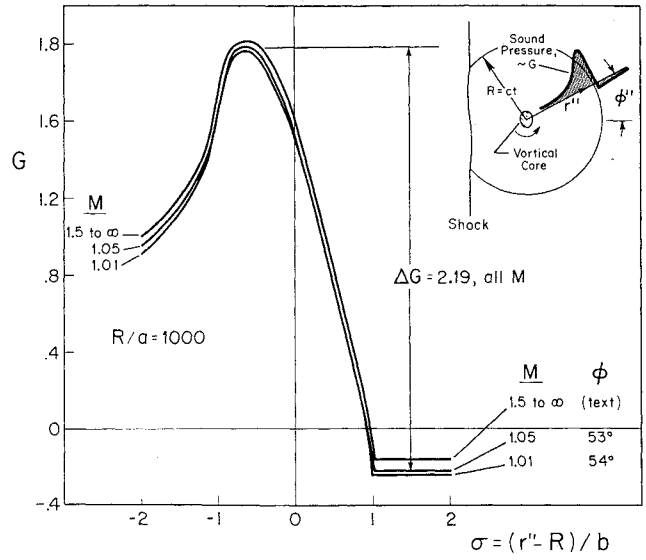

Fig. 7 Normalized radial sound pressure profile G (evaluated at first peak of $(b/a)^{1/2}\hat{P}J$ vs ϕ'', Figs. 6). Upstream M as in Figs. 6.

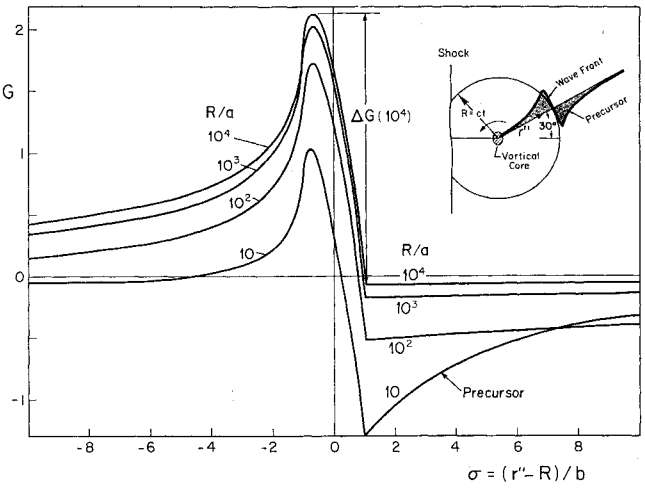

Fig. 8 Normalized radial sound pressure profile G evaluated at $\phi''=30$ deg, for $R/a=10$, 10^2 10^3, 10^4. Upstream $M=1.25$.

Variation with Nominal Radius $R=ct$

Radial pressure profiles $G(\sigma)$ for $R/a=10$, 10^2, 10^3, and 10^4 are shown in Fig. 8. These refer to a fixed flow Mach number $M=1.25$ and fixed angle $\phi''=30$ deg. The jump ΔG in the vicinity of $r''=R$ ($\sigma=0$) defines what we have termed the cylindrical wave "front." More precisely, the profile minimum at $r''=R+b(\phi'')$ ($\sigma=1$) describes the "front": the wave has had time to propagate exactly this far in direction ϕ'' since the relevant part of the incident vortex core (of radius a) first touched the shock. (The time $t=R/c$ is taken as zero when the center of the vortex core transits the shock plane.)

The striking feature of Fig. 8 is the failure of the sound pressure to drop to zero at the wave front ($\sigma=1$) and beyond: there is a *precursor* surrounding the vorticity-driven wave. It is found that at $\sigma=1$ this precursor [with cancelled-out $(a/R)^{1/2}$ factor restored] scales as R^{-1}.

The contribution of *evanescent* waves, not included in the calculated pressure field, was evaluated numerically for a few cases for comparison. Their contribution varies smoothly with r'', adding nothing to the pressure *jump* $\sim\Delta G$ at $r''\simeq R$. However, it does add very significantly to the magnitude of the negative precursor (from about 12% at $\phi''=16$ deg to almost threefold at $\phi''=105$ deg, diminishing for larger ϕ''); the contribution to the precursor scales like R^{-1} at $\sigma=1$. The inclusion of these waves (involving double

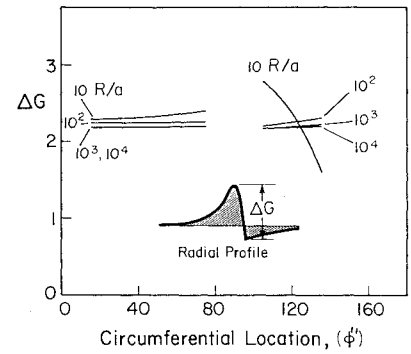

Fig. 9 Radial pressure jump ΔG at wave front ($r''\simeq R$) vs azimuth angle ϕ'' for various nominal radii R (or various times $t=R/c$). Upstream $M=1.25$.

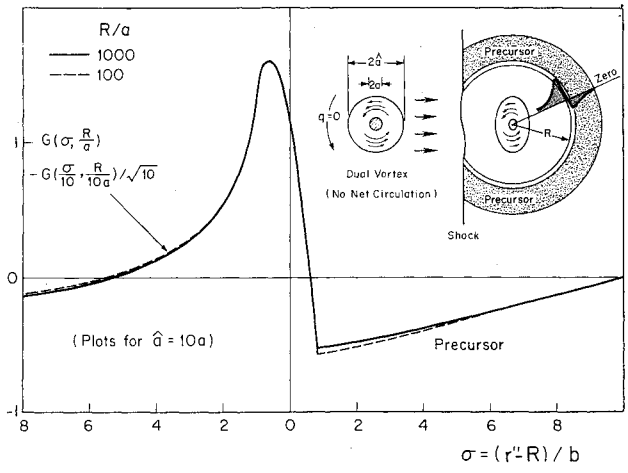

Fig. 10 Special model of vortex/shock interaction to explore precursor to main vortex-driven sound wave. Dual vortex with *zero induced velocity* for $r\geq\hat{a}$ ($\hat{a}=10a$) is convected through shock. Radial pressure profile shows this precursor to be strictly bounded, obeying causality: its outer limit is dictated by time of first contact of the dual vortex [region of nonzero velocity field $q(r)$] with the shock.

numerical integration with one running upper limit) would make relatively great demands for computer time and is of questionable accuracy. We justify their omission on that account and also because our primary interest is in the propagating sound wave characterized by the jump ΔG.

By contrast to the precursor, $(a/R)^{1/2}\Delta G$ scales as $R^{-1/2}$, since ΔG is essentially constant with R for $R/a = 10^2$ to 10^4. Figure 9 shows this, as well as a near constancy with ϕ'', for the single Mach number $M = 1.25$. (For the fixed large value $R/a = 10^3$, Fig. 7 showed constancy of ΔG with M at specified values of ϕ''.)

Comparative Profile of Impulsive Line Source

It will be of interest to make comparisons with an impulsive two-dimensional point source of sound initiated at $t = 0$. The sound field (Green's function) is[19]

$$p = \text{const}/\sqrt{R^2 - r''^2}, \quad R = ct \tag{14}$$

For point r'' near the wave front R ($R - r'' \ll R$), this may be approximated as

$$p = \text{const}/\sqrt{2R}\sqrt{R - r''} \tag{15}$$

Thus, for fixed $R - r''$ (or fixed σ in our plots), p is proportional to $R^{-1/2}$; this is compatible with the constancy of ΔG with R cited in Fig. 9.

If, on the other hand, R is fixed (thus fixing the time), Eq. (15) gives a snapshot of a radial pressure profile. Numerical evaluation shows a fair agreement between this idealized profile and those resulting from the shock/vortex interaction (Figs. 7 and 8). Equation (15) shows p rising slightly faster with σ ($\sim R - r''$) and with a square root singularity replacing the rounded peak. Departing from the unreality of a point source to a small but finite source ($\sim$ the vortex core) should eliminate the singularity.

The Precursor Wave

None of this applies to the *precursor waves* (the negative dips of Figs. 7 and 8); these decay at $\sigma = 1$ like R^{-1} rather than $R^{-1/2}$. Physically, we would explain a precursor wave as arising from the potential flow surrounding the vortex core. Since this extends to infinity, it encounters the shock an infinite time in advance of the core. The large-scale pressure field generated by the encounter "starts" with infinitesimal amplitude and grows as the core approaches the shock from upstream.

A nice test of this notion can be made via a composite (dual) vortex. This consists of uniform counterclockwise vorticity of total circulation Γ over an area πa^2 as before. Superimposed is uniform clockwise vorticity, of total circulation $-\Gamma$, over a much larger area $\pi \hat{a}^2$. It is easily shown that the induced velocity field is clockwise over the entire area $\pi \hat{a}^2$: it peaks at radius a and decays to zero at radius $\hat{a}$ *and everywhere beyond.* Thus, if our explanation fits, any precursor surrounding the emission from the core πa^2 should have a *finite* radial extent: it should not extend to infinity.

As an example, we may take $R/a = 100$ and $R/\hat{a} = 10$. Then our previous computer computations may be applied, but with $R/a = 10$ reinterpreted as $R/\hat{a}$. Further specifications are $M = 1.25$ and $\phi'' = 30$ deg. The resulting radial profile $G(\sigma)$, obtained by superposition, is shown in Fig. 10; also shown is the case $R/a = 1000$, $R/\hat{a} = 100$. The comparison with previous figures is striking (see especially Fig. 8): instead of extending asymptotically to zero at infinity, the precursor decays to exactly zero at $\sigma = 10$ and remains zero for all larger values.

This result is noteworthy for two reasons: 1) it supports our concept of the origin of the precursor wave and 2) it demonstrates that the calculations obey causality: no sound field is generated in advance of the earliest encounter of a disturbance (the vortex-induced velocity field) with the shock.

Comparison with Experiment

The circumstances addressed by the theory may be approached experimentally in a shock tube. A shock propagates past an airfoil at an angle of attack and the drift flow generates a starting vortex that rolls up behind the trailing edge: this approximates our columnar vortex. The shock reflects at the solid end of the shock tube and returns to pass over the vortex. Schlieren photographs (i.e., Fig. 1)[7] show clearly the cylindrical sound wave generated by the encounter.

The first experiment of this kind was carried out by Hollingsworth and Richards,[1] who initiated theoretical interest in the problem.[2] This was carefully repeated by Dosanjh and Weeks,[7] with the addition of interferometric photography. (See also the later Ref. 20.) This allowed them to deduce quantitatively the circumferential density variation from fringe shifts. More precisely, they evaluated, in effect, the

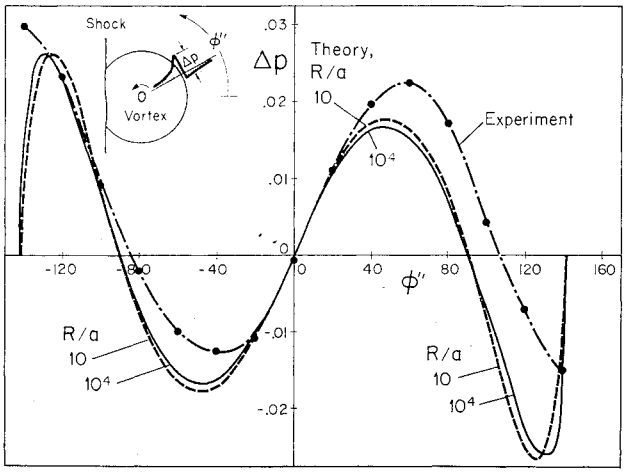

Fig. 11 Vortex/shock interaction. Direct comparison of present theory with experiment as reported by Dosanjh and Weeks[7]: variation with ϕ'' of pressure jump Δp (normalized by ambient pressure) at $r'' \simeq R = ct$ in cylindrical sound wave; experimental $R/a = 10.055$, $M = 1.29$. (See text for other parameters.)

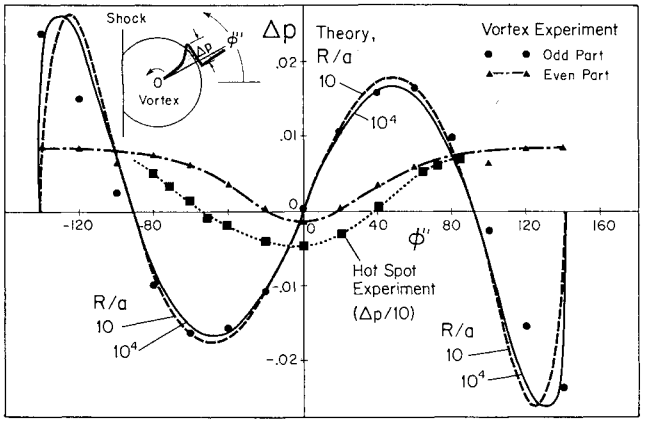

Fig. 12 Vortex/shock interaction. Comparison of present theory with *odd* (antisymmetric) *part* of experimental curve of Dosanjh and Weeks[7]: variation with ϕ'' of pressure jump Δp (normalized by ambient pressure) at $r'' \simeq R = ct$ in cylindrical sound wave; experimental $R/a = 10.055$, $M = 1.29$. *Even part* of vortex/shock interaction curve is seen to have qualitative resemblance to *hot-spot/shock* interaction curve.[21]

nondimensional density jump $\Delta\rho$ (expressed as fraction of ambient) at the cylindrical wave front near R as a function of ϕ. They converted this to a nondimensional pressure jump Δp by means of the isentropic approximation $\Delta p = \gamma\Delta\rho$.

[The interaction process is not, however, quite isentropic according to the theory. Superposed on the shear waves dq' of Fig. 5 are entropy waves that are not shown.[4,8] As a matter of interest, some calculations have been made of the contribution of these entropy waves to the density field. It was found to be quite small, averaging less than 2.5% for $M=1.25$ and $R/a=10$, 10^2, and 10^3. More importantly, this entropy contribution to ρ varies smoothly with radial distance: this is no radial jump in entropy where the pressure exhibits the jump Δp ($\sim\Delta G$). Thus, the isentropic approximation for Δp is very close.]

We now restate the theoretical prediction [Eq. (12)] to refer to the pressure jump at the wave front normalized as ΔG in Figs. 7-10; with use of Eq. (6), it reads

$$\Delta p(\phi'') = \underbrace{\left[\frac{2^{1/2}q_{\max}}{\pi U_A}\left(\frac{a}{R}\right)^{1/2}\right]}_{\text{const}}\underbrace{\Delta G(\phi'';R/a)}_{\text{radial}}\underbrace{\left(\frac{b}{a}\right)^{1/2}_{\phi''}P(\phi'')J(\phi'')}_{\text{circumferential}} \tag{16}$$

At a given Mach number the strength factor [ ] is constant at a fixed time t ($=R/c$) and the circumferential factor depends uniquely on ϕ''. Dosanjh and Weeks[7] give for the circumstances of their experiment: $U_A=504.7$ m/s (1656 ft/s), $q_{\max}=153.6$ m/s (581 ft/s), $R/a=10.005$, and $M=1.29$. Thus, the numerically predicted circumferential profile of Δp is

$$\Delta p(\phi'') = 0.0996\Delta G\left(\phi''; \frac{R}{a}\right)\left(\frac{b}{a}\right)^{1/2}_{\phi''}\hat{P}(\phi'')J(\phi'') \tag{17}$$

In applying this the circumferential factor $(b/a)^{1/2}\hat{P}J$, which is sensitive to Mach number (Fig. 6), was calculated for the actual case $M=1.29$; the values of ΔG, which are relatively insensitive (Fig. 7), were taken for $M=1.25$ (Fig. 9).

The theory and experiment are compared directly in Fig. 11. The curves are fairly similar, but show a relative shift. The theoretical curve is exactly antisymmetric, but the experimental one only approximately so. We attribute the departure from antisymmetry to the interaction of the vortex *pressure* field with the shock. Although second order in velocity ($\sim q^2_{\max}$), it is strong enough to appear in schileren photos. This depressed pressure zone can be expected to interact with the shock; being axisymmetric it would yield a sound wave with symmetry in + or $-\phi''$. The resultant circumferential Δp should then be a superposition of symmetric and antisymmetric components: that is, a sum of even and odd functions of ϕ''.

The present theory, being linear, completely ignores the second-order pressure field of the vortex and its effects. Thus, the theory refers only to that part of the experimental $\Delta p(\phi'')$ that is an odd function of ϕ''. On writing

$$\Delta p(\phi'') = \Delta p_E(\phi'') + \Delta p_0(\phi'')$$
$$\Delta p(-\phi'') = \Delta p_E(\phi'') - \Delta p_0(\phi'') \tag{18}$$

the even and odd parts, Δp_E and Δp_0, respectively, can be obtained uniquely by summing and differencing. In this fashion, the odd part of the experimental $\Delta p(\phi'')$ was obtained and is plotted in Fig. 12. For comparison, the prediction (17) is also plotted, not only for the correct $R/a\simeq 10$, but also with ΔG evaluated for $R/a=10^4$ (R/a is still held at 10.055 in the numerical factor). It is seen that the agreement of theory with experiment is vastly improved compared with Fig. 11: it is excellent for $|\phi''|<90$ deg. Although the experimental $R/a\simeq 10$, comparable agreement is obtained for the extreme far-field (late-time) condition $R/a=10^4$ in evaluating ΔG.

Above $\phi=90$ deg the agreement deteriorates and the experimental curve, as presented, fails to show the theoretical sharp drop to zero at $\phi''=\phi''_{cr}$ ($=142.3$ deg). In discussions with Weeks[23] he expressed the view that there is a possibility that the large $|\Delta p|$ interferometric measurements near ϕ''_{cr} could have been subject to error owing to refraction by the large density gradients. The schlieren photograph in Fig. 1 does seem to show a drop toward zero (lower left) as $\phi''\to-\phi''_{cr}$.

Hamernik and Dosanjh[21] have carried out a similar experiment in which a round hot spot (in two dimensions, due to an exploding wire) passes through a planar shock. This produces a cylindrical sound wave in which Δp is an *even* function of ϕ''. In this aspect the behavior resembles what we have argued should be the case for the pressure depression at the core of the vortex. As a matter of interest, their curve of Δp (scaled down tenfold) has been plotted on Fig. 12 as well. There is qualitative similarity with the even part of $\Delta p(\phi'')$ for the experimental vortex/shock interaction, despite the difference in the initiation (hot spot rather than pressure spot).

We conclude with some remarks on another nonlinear process. The experimental sound wave when the radius has grown to $R/a\simeq 10$ is still acoustically very intense: Δp corresponds to 170.8 dB at $\phi''=-\phi''_{cr}$ and 160.4 dB at $\phi''=58$ deg (both compression).[7] Thus, the wave must have experienced substantial nonlinear distortion during its propagation outward from the vortex core. The effect, well documented in sonic boom theory vs experiment,[22] would be expected to steepen and localize the compression and to spread out the rarefaction. The steepening does seem to appear in Fig. 1, in the stronger compression zone (arrow in the figure), but not in the one peaking at 58 deg. The figure does seem to show a precursor as predicted, but it seems rather localized (a steepening effect) in a narrow zone just outside the nominal radius R. The expected spreading in rarefaction zones is hard to discern.

Appendix: Equations and Definitions for Evaluation of Shock-Interaction Transfer Function $\hat{P}$, Jacobian J, and Factor $(b/a)^{1/2}$

The equations listed below apply only for the range of *nonevanescent* waves (W of Fig. 4 $\geq$ sound speed); the calculated results plotted herein are limited to this regime. These functions are equivalent to those of the basic Refs. 4 and 8; however, a number are in different form in order to provide a more convenient sequencing for numerical evaluation. The equations are valid, in general, *only for the positive range of the angles*. The ratio of specific heats γ has been taken as 1.4.

M = specified
α'' = specified
$m = 6M^2/(5+M^2)$
$M_1 = (5+M^2)^{1/2}/(7M^2-1)^{1/2}$
$\tilde{W} = \dfrac{W}{c} = \left[1+\left(\dfrac{M_1+\cos\alpha''}{\sin\alpha''}\right)^2\right]^{1/2}$
$\mu = \sin^{-1}(1/\tilde{W})$
$\alpha' = \alpha''-\mu$
$\alpha = \tan^{-1}(m\tan\alpha')$
$b/a = \sin\alpha''/\sin\alpha$ (subscript ϕ or ϕ'' implies evaluation at $\alpha''=\phi''$)

$$\hat{P}(\alpha'') = -\frac{7m\Pi\csc\alpha'}{6m-1}$$

$$\hat{P}(\phi'') = \hat{P}(\alpha''), \text{ for } \alpha'' = \phi''$$

$$\Pi = \frac{\sin\alpha\sin\mu}{m\sin\alpha''}\left[\left(\frac{C'+GF'}{E'+GD'}\right)D' - F'\right]$$

$$C' = (1/3)m - 2[1+(m-1)\sin^2\alpha']$$
$$D' = (m-1)[1+(m-1)\sin^2\alpha']$$
$$E' = (m-1)F'/2 - [1+(2/3)m]\cot\alpha'$$
$$F' = (m-1)\sin 2\alpha'$$
$$G = -\cot\alpha'' \text{ [in } \Pi \text{ equation only, not to be confused with } G(\sigma)]$$

$$J(\alpha'') = \frac{(\sin^2\alpha)\tan\alpha'}{m\sin^2\alpha'(\tan\alpha'+\tan\mu)}$$

$$J(\phi'') = J(\alpha''), \text{ for } \alpha'' = \phi''$$

Acknowledgments

I am indebted to Dr. David Kopriva of the Massachusetts Institute of Technology for reviving my interest in this problem. What in an early stage was a collaborative effort to compare analytical and computational results has evolved into separate studies. Support at the University of Toronto was aided by a grant from the Natural Sciences and Engineering Research Council of Canada and at the NASA Langley Research Center by tenure as a Distinguished Research Associate.

References

[1]Hollingsworth, M. A. and Richards, E. J., "A Schlieren Study of the Interaction Between a Vortex and a Shock Wave in a Shock Tube," British Aeronautical Research Council, Rept. 17 985, FM 2323, Nov. 1955.

[2]Hollingsworth, M. A. and Richards, E. J., "On the Sound Generated by the Interaction of a Vortex and a Shock Wave," British Aeronautical Research Council, Rept. 18 257, FM 2371, Feb. 1956.

[3]Powell, A., "On the Mechanism and Reduction of Choked Jet Noise," British Aeronautical Research Council, Rept. 15 623, FM 1858, Dec. 1952.

[4]Ribner, H. S., "Shock-Turbulence Interaction and the Generation of Noise," NACA TN 3255, July 1954, and NACA Rept. 1233, 1955.

[5]Harper-Bourne, M. and Fisher, M. J., "The Noise from Shock Waves in Supersonic Jets," *Noise Mechanisms*, AGARD CP-131, 1973, pp. 11-1—11-13.

[6]Pao, S. P. and Seiner, J. M., "Shock Associated Noise in Supersonic Jets," *AIAA Journal*, Vol. 21, May 1983, pp. 687-693.

[7]Dosanjh, D. S. and Weeks, T. M., "Interaction of a Starting Vortex as Well as a Vortex Street with a Travelling Shock Wave," *AIAA Journal*, Vol. 3, Feb. 1965, pp. 216-223.

[8]Ribner, H. S., "Convection of a Pattern of Vorticity Through a Shock Wave," NASA TN 2864, Jan. 1953, and NACA Rept. 1164, 1954.

[9]Moore, F. K., "Unsteady Oblique Interaction of a Shock Wave with a Plane Disturbance," NACA TN 2879, 1953 and NACA Rept. 1165, 1954.

[10]Chang, C. T., "Interaction of a Plane Shock and Oblique Plane Disturbances with Special Reference to Entropy Waves," *Journal of the Aeronautical Sciences*, Sept. 1957, pp. 675-682.

[11]Kerrebrock, J. L., "The Interaction of Flow Discontinuities with Small Disturbances in a Compressible Fluid," Ph.D. Thesis, California Institute of Technology, Pasadena, 1956.

[12]Ram, G. S. and Ribner, H. S., "The Sound Generated by Interaction of a Single Vortex with a Shock Wave," *Heat Transfer and Fluid Mechanics Institute*, 1957, pp. 1-21; also, Ribner, H. S., University of Toronto, Institute for Aerospace Studies, UTIA Rept. 61, 1959.

[13]Lighthill, M. J., "On Sound Generated Aerodynamically, I: General Theory," *Proceedings of the Royal Society of London*, Vol. A211, 1952, pp. 564-587.

[14]Curle, N., "The Influence of Solid Boundaries Upon Aerodynamic Sound," *Proceedings of the Royal Society of London*, Vol. A231, 1955, pp. 505-514.

[15]Weeks, T. M. and Dosanjh, D. S., "Sound Generated by Shock-Vortex Interaction," *AIAA Journal*, Vol. 5, April 1967, pp. 660-669.

[16]Pao, S. P. and Salas, M. D., "A Numerical Study of Two-Dimensional Shock-Vortex Interaction," AIAA Paper 81-1205, June 1981.

[17]Zang, T. A., Hussain, M. Y., and Bushnell, D. M., "Numerical Computations of Turbulence Amplification in Shock-Wave Interactions," *AIAA Journal*, Vol. 22, Jan. 1984, pp. 13-21.

[18]Watson, G. N., *A Treatise on the Theory of Bessel Functions*, Cambridge University Press, London; Macmillan Co., New York, 1945, p. 405.

[19]Morse, P. M. and Feshbach, H., *Methods of Theoretical Physics, Part II*, McGraw-Hill Book Co., New York, 1953, p. 1363.

[20]Naumann, A. and Hermanns, E., *Noise Mechanisms*, AGARD CP-131, 1973, pp. 23-1—23-10.

[21]Hamernik, R. P. and Dosanjh, D. S., "Generation of Acoustic Waves During the Passage of a Shock Wave Through a Heated Gaseous Element," *Journal of the Acoustical Society of America*, Vol. 53, No. 3, 1973, pp. 921-925.

[22]Carlson, H. W. and Maglieri, D. J., "Review of Sonic-Boom Generation Theory and Prediction Methods," *Journal of the Acoustical Society of America*, Vol. 51, 1972, pp. 675-685.

[23]Weeks, T. M., Private communication.